



HAL
open science

Island formation in submonolayer epitaxy

Lei-Han Tang

► **To cite this version:**

Lei-Han Tang. Island formation in submonolayer epitaxy. Journal de Physique I, 1993, 3 (4), pp.935-950. 10.1051/jp1:1993174 . jpa-00246774

HAL Id: jpa-00246774

<https://hal.science/jpa-00246774>

Submitted on 4 Feb 2008

HAL is a multi-disciplinary open access archive for the deposit and dissemination of scientific research documents, whether they are published or not. The documents may come from teaching and research institutions in France or abroad, or from public or private research centers.

L'archive ouverte pluridisciplinaire **HAL**, est destinée au dépôt et à la diffusion de documents scientifiques de niveau recherche, publiés ou non, émanant des établissements d'enseignement et de recherche français ou étrangers, des laboratoires publics ou privés.

Classification

Physics Abstracts

68.55 — 61.50C — 68.10J

Island formation in submonolayer epitaxy

Lei-Han Tang

Institut für Theoretische Physik, Universität zu Köln, Zùlpicher Str. 77, D-5000 Köln 41, Germany

(Received 27 October 1992, accepted in final form 13 November 1992)

Abstract. — A minimal model for molecular-beam-epitaxy in the submonolayer at room temperature is investigated by simulations and analytically. Aggregation of diffusing monomers leads to immobile islands which further grow by absorbing deposited and diffusing atoms. In the intermediate stage of growth, islands assume a fractal shape similar to diffusion-limited-aggregates. It is shown that the maximum density of islands in the submonolayer decreases approximately as a $1/3$ -power of the beam intensity F , in agreement with a prediction based on rate equations. A detailed analysis of adatom-adatom and adatom-island collisions explains some discrepancies between simulation data and simple rate-equation results.

1. Introduction.

The fundamental physical process of molecular beam epitaxy (MBE) involves nucleation, growth and coalescence of two-dimensional (2D) islands in an environment of supersaturated lattice-gas on the film surface created by the beam [1-9]. An important lengthscale which emerges in the growth on a high-symmetry substrate is the typical distance ℓ between islands (or steps). A large ℓ is obviously desirable for device applications. Under favourable growth conditions, ℓ can be of the order of a few thousand angstroms. In general ℓ increases with decreasing beam intensity F . The precise relationship between ℓ and F depends on the details of the dynamics of adatom diffusion, adatom-adatom interaction and the adsorption and desorption of adatoms at the island edges [3-9]. At elevated temperatures (~ 500 °C), desorption of surface atoms into the vapor may also be relevant [9].

Several theoretical approaches have been advanced to address specific aspects of surface diffusion and island formation in MBE [3-8]. In the case of high supersaturation, where there is essentially no energy barrier for the formation of stable islands, a quantitative theory which relates the island size to the beam intensity and adatom and cluster diffusion constants appears feasible [3, 4, 8]. However, contradictory results exist in the literature [10, 11]. Recent simulation studies by Mo *et al.* [12], while supporting an earlier prediction by Stoyanov and Kashchiev [3], have not explored consequences of fractal islands that appear in diffusion-limited island growth. These fractal shapes have been observed recently for Au on Ru at room temperature by Hwang *et al.* [13].

In this paper we present a detailed analytical and simulational study of a minimal model for MBE [8, 12]. The model, which will be explained in detail in the next section, assumes that atoms stick on contact, and that all but monomers are immobile. Such a model is reasonable for MBE at room temperature, where pair breaking can be safely ignored during the typical laboratory time of the order of 1 min. We shall restrict ourselves to the submonolayer coverage, where multilayer transport plays no role. This regime is an ideal playground for measuring surface diffusion constant of adatoms, as has been done in several experiments [1, 10, 14]. In general our results agree with those of Stoyanov and Kashchiev, as reported briefly in reference [8]. However, significant deviations from the behavior predicted by simple rate equations are also observed. We show here that some of these deviations arise from the logarithmic anomaly of 2D random walks.

It is worth mentioning at this point the connection between this work and previous studies of kinetic roughening of growing surfaces in general [15-17] and that of film surface in MBE in particular [18-22]. The main focus of previous studies has been the self-affinity of surface roughness and the identification of various universality classes. The models constructed for that purpose are presumably applicable on a coarse-grained level, e.g., treating each island as a single block. The present and other recent works [8, 23] can be thought of as part of an on-going program to establish the missing link between the vast literature on surface diffusion on the atomic level and the modern theory of kinetic roughening, thereby offering a quantitative theory of kinetic roughening in MBE. On a technical level, our model belongs to the class of diffusion-aggregation-growth models reviewed by Herrmann in reference [24]. However, it differs from the cluster-cluster aggregation models [25, 26] in that atoms are continuously created on the surface during growth, rather than fixed at a given density.

The paper is organized as follows. In section 2 we define the model and summarize previous analytical results based on rate equations. Section 3 contains a general description of various processes during growth as observed in our simulations and the numerical results for the adatom and island densities at various coverages and deposition rates. Section 4 contains a calculation which takes into account logarithmic corrections to the collision rates, as well as a few other effects neglected in the rate equations. The calculation yields a significantly better fit to our simulation data at early times. A summary is given in section 5. A few mathematical details are relegated to the three appendices.

2. The model and rate equations.

2.1 THE MODEL. — A minimal model for MBE on an initially flat substrate can be defined as follows. Starting at $t = 0$, atoms are randomly and continuously deposited onto a square lattice at a rate F per site. An adatom (or synonymously, a monomer) performs nearest neighbor hopping on the lattice at a rate $4D$ in any of the four possible directions. Here D is the adatom diffusion constant in the usual sense, taking the lattice constant to be the unit of length. An *island* is a cluster of atoms on the surface, connected by nearest neighbor bonds. An adatom becomes immobile when it hits another adatom or the edge of an existing island. (This further implies that all but monomers are stable and immobile.) Adatoms deposited on top of existing atoms diffuse in the same way as those in the layer below. They are incorporated into the film through collisions with atoms in the same layer or by falling onto a lower level when it wanders out the edge of the terrace. No energy barrier is assumed for the latter process. In addition, an atom created on top of another adatom immediately forms an immobile dimer with that adatom in the lower level. In this paper we focus on the submonolayer régime, where the total number of deposited atoms is less than the number of sites on the square lattice. Due to statistical fluctuations, however, there can be a small population of atoms in the second layer. The model as we defined it can be used for multilayer growth, too.

It is clear from the above definition that there are only two basic time scales in the model, the typical nearest neighbor hopping time $1/(4D)$ and the layer completion time $1/F$. If we choose $1/(4D)$ to be the unit of time, all physical quantities will depend only on the ratio $4D/F$. Nevertheless, we shall keep $4D$ in our expressions to facilitate comparison with other works. The unit of length, however, is taken to be the lattice constant rather than e.g. cm.

2.2 RATE EQUATIONS. — The general features of island formation in the submonolayer regime are captured by the rate equations, (see e.g. Refs. [2], [3] and [8])

$$dN/dt = 4D\rho^2, \quad (1a)$$

$$d\rho/dt = F - 4D\rho(2\rho + N), \quad (1b)$$

with the initial condition $\rho(0) = N(0) = 0$. Here ρ and N are adatom and island densities, respectively. The factor 2 in (1b) comes from the fact that two adatoms are eliminated in an adatom-adatom collision.

The natural length and time scales of (1) are given by

$$\ell_1 = (4D/F)^{1/4}, \quad t_1 = (4DF)^{-1/2} \quad (2)$$

Introducing the dimensionless quantities $\hat{\rho} = \ell_1^2 \rho$, $\hat{N} = \ell_1^2 N$, and $\hat{t} = t/t_1$, equations (1) become

$$d\hat{N}/d\hat{t} = \hat{\rho}^2, \quad (3a)$$

$$d\hat{\rho}/d\hat{t} = 1 - \hat{\rho}(2\hat{\rho} + \hat{N}). \quad (3b)$$

Solution to (1) can thus be expressed in the scaling form,

$$N(t) = (F/4D)^{1/2} \hat{N}(t\sqrt{4DF}), \quad (4a)$$

$$\rho(t) = (F/4D)^{1/2} \hat{\rho}(t\sqrt{4DF}). \quad (4b)$$

The short and long time behavior of the solution to (3) can be easily worked out. For $\hat{t} \ll 1$, we have

$$\hat{\rho} \approx \hat{t}, \quad \hat{N} \approx \frac{1}{3} \hat{t}^3, \quad (5)$$

while for $\hat{t} \gg 1$,

$$\hat{N} \approx 1/\hat{\rho} \approx (3\hat{t})^{1/3} \quad (6)$$

The density of islands at t_1 is of the order

$$N_1 \approx \ell_1^{-2} = (F/4D)^{1/2} \quad (7)$$

This is also roughly the density of adatoms at this time. In references [10] and [11] it was assumed that nucleation stops when the island density reaches this value. However, growth of N can only be terminated by coalescence. For compact islands, this takes place when the coverage reaches a significant fraction of the total area of the surface, say $Ft_2 = 1/4$. Equation (6) then yields

$$N_{\max} \equiv N(t_2) \approx (F/4D)^{1/3} \quad (8)$$

This is the result of Stoyanov and Kashchiev [3].

3. Simulation.

The simulation results reported below are for a system of 256^2 sites with periodic boundary conditions. The ratio of diffusion to deposition rates varies from 32 to about 4×10^6 in powers of 2, i.e., $4 D/F = 2^n$, $n = 5, \dots, 22$. Since the maximum size of islands in our simulation before coalescence is less than about 20 lattice constants, and the typical diffusion length of monomers is of the same order except at very early times, finite-size corrections are insignificant up to $4 D/F \sim 10^6$. The statistics is made over about 100 samples in each case. The adatom density $\rho(t)$ and the density of islands $N(t)$ are measured at uniform time intervals up to half coverage. In addition, we have recorded the average mass and radius of each island during growth. The Hoshen-Kopelman algorithm [27] is used for cluster counting.

3.1 THREE STAGES OF GROWTH. — Starting from a flat substrate, the formation of islands in the first layer takes place in three stages, the first and the second according to the relative population of adatoms and islands, and the third when coalescence becomes significant. Figure 1 shows a sequence of snapshots of a 64^2 system at $4 D/F = 65\,536$. The coverage

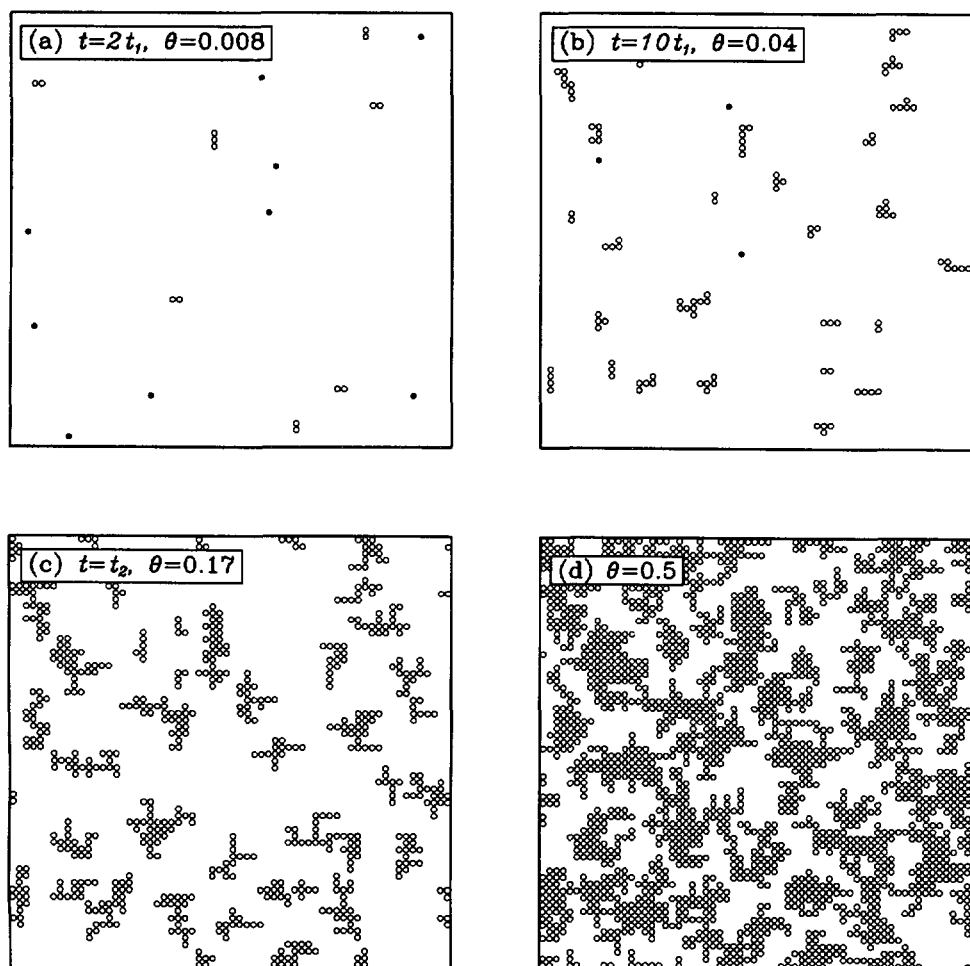


Fig. 1. — Top views of a 64^2 lattice showing different stages of growth. Adatoms are indicated by solid circles. Here $4 D/F = 65\,536$.

θ is indicated on each plot. Figure 1a corresponds to the end of the first stage ($t < t_1$), where the number of islands catches up with the number of adatoms. Most islands at this time are still dimers. In the second stage $t_1 \leq t \leq t_2$, as shown in figure 1b, there are much more islands than adatoms. Therefore most adatoms disappear through collision with islands. However, the number of islands continues to increase. Figure 1c marks the beginning of the third stage ($t > t_2$), the coalescence of islands. The size of islands at this time is comparable to the spacing between them. Finally, figure 1d shows the system at half-coverage. The adlayer consists of an intricate network of densely-packed regions. The characteristic length of this network is about the same as the average distance between islands in figure 1c.

The picture described above is typical for all values of $4 D/F$ greater than about 100. For smaller values of $4 D/F$, t_1 is not much smaller than t_2 , and islands before coalescence contain no more than a few atoms. Consequently the three-stage description loses its meaning. This can be seen from figure 2, where we plotted the density of islands i) $N = N_1$, when it is equal to the density of adatoms at $t \approx t_1$ (open circles), and ii) $N = N_{\max}$, when it reaches a maximum at $t = t_2$ (solid circles). For $4 D/F \approx 4 \times 10^6$, N_{\max} is about 6 times N_1 , while at $4 D/F = 128$ the ratio is less than 2. More importantly, N_{\max} follows essentially the 1/3-law at large values of $4 D/F$ as predicted by equation (8), while N_1 decreases faster with increasing $4 D/F$. Deviations from the simple expressions (7) and (8) are also evident. They will be examined in section 4.

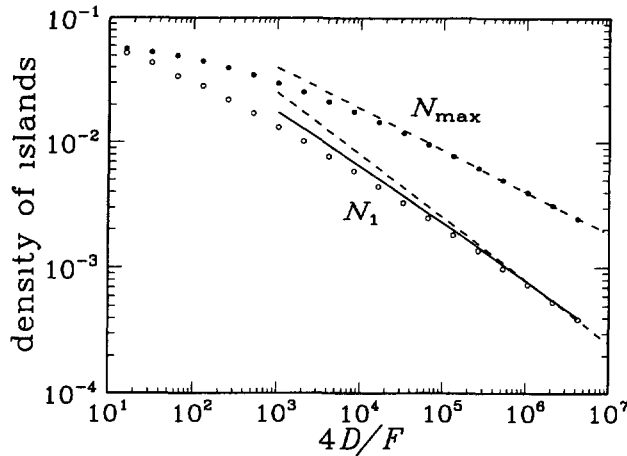


Fig. 2. — The density of islands as a function of the inverse deposition rate $4 D/F$. N_1 (open circles) is the density of islands when it is equal to the density of adatoms. N_{\max} (solid circles) is the maximum island density. Two lines representing a powerlaw behavior $N_{\max} \sim (4 D/F)^{-1/3}$ (dashed-dotted) and $N_{\max} \sim (4 D/F)^{-1/2}$ (dashed) are drawn for comparison. The solid line corresponds to equation (15).

Figure 3 shows the full time dependence of ρ and N for $4 D/F \geq 1\,024$, scaled according to equation (4). The numerical solution to (3) is given by the two dashed lines. The qualitative features of the data are well represented by the solution to the rate equations. At early times $t \ll t_1$, $\rho(t)$ increases linearly with t while $N(t)$ increases roughly as a power-law of t with an exponent close to the value 3 as in (5). The adatom density $\rho(t)$ reaches a maximum shortly before the two curves cross around $2 t_1$. For the values of $4 D/F$ considered here the crossing point is between $1.5 t_1$ and $2.5 t_1$. For $t > t_1$, $\rho(t)$ continues to decrease while $N(t)$ crosses over to a much slower growth than at earlier times. At a much later time

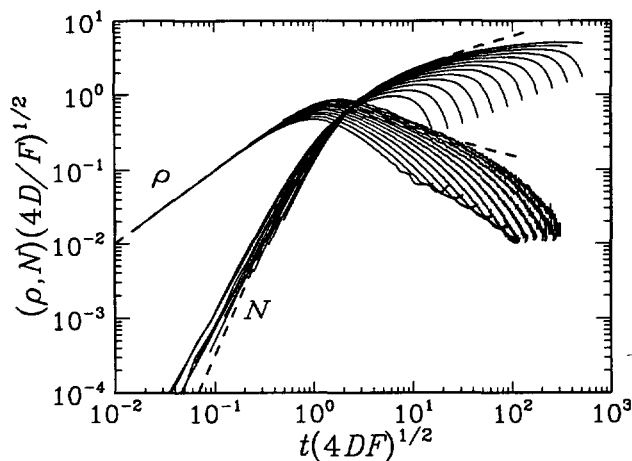


Fig. 3. — Scaled density of adatoms $\rho \sqrt{4 D/F}$ and of islands $N \sqrt{4 D/F}$ as a function of scaled time $t \sqrt{4 D F}$. Each curve corresponds to a given value of $4 D/F = 2^n$, $n = 10, \dots, 22$. On the right half of the plot, $4 D/F$ increases upwards. Data for N are shown up to half coverage except for $n = 21$ and 22 . The dashed lines correspond to the solution to the rate equations (3).

t_2 , $N(t)$ reaches its maximum value N_{\max} . However, the absence of a complete data collapse up to t_2 indicates that the scaling forms (4) are not exact.

3.2 FRACTAL ISLANDS. — The islands shown in figure 1c have a fractal shape. Since most of the atoms on an island up to this time arrived as random walkers, it is not surprising that our islands resemble clusters obtained from diffusion-limited-aggregation (DLA) [28]. Figure 4 shows the average mass per cluster as a function of the average radius of gyration up to $t = t_2$. Each curve corresponds to a given value of $4 D/F \geq 1\ 024$. The lower envelope of the curves appears to converge to a power-law with the fractal dimension $d_f = 1.72$ of DLA

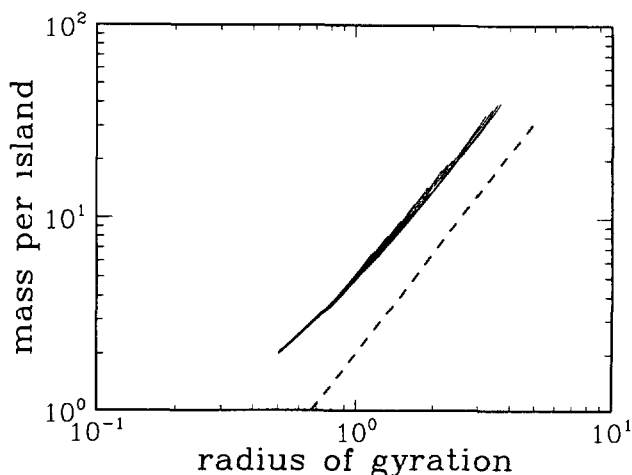


Fig. 4. — Average mass per island versus average radius of gyration for $t < t_2$. Each curve corresponds to a given value of $4 D/F$. The dashed line shows a power-law with an exponent $d_f = 1.72$ as for the diffusion-limited aggregation.

(dashed line). However, as t increases towards t_2 , the lines curve upwards, indicating that islands become more compact.

4. Random walks revisited.

The rate equations (1) neglect completely the spatial and temporal correlations of adatom and island positions. In this sense they are mean-field equations. Furthermore, islands are treated as point objects, which is a good approximation only when their size is much smaller than the spacing between them. We discuss here possible improvements based on a more detailed analysis of adatom diffusion, as proposed first in reference [8] in a similar context.

4.1 VERY SHORT TIMES. — In the regime $t \ll t_1$, each adatom explores a territory much smaller than the area per adatom or island. A stable pair forms when two such territories overlap. The probability that three or more adatoms explore the same territory is much smaller.

Within the approximation that the pair-formation rate in a dilute lattice-gas of adatoms is given by a linear superposition of the collision rate of *independent* random walkers, standard results for 2D random walks can be applied [29]. These results are rederived in appendices A and B for completeness, tailored to our needs. In terms of the probability $P(t - \tau)$ that an adatom landed at time $\tau < t$ collides with any of the preexisting adatoms of unit density within a time interval $t - \tau$, the number of pairs formed in a time t is given by

$$N(t) = \int_0^t F d\tau \rho(\tau) P(t - \tau). \quad (9a)$$

Similarly, we write the density of adatoms at time t as

$$\rho(t) = Ft - 2 \int_0^t F d\tau \rho(\tau) P(t - \tau) - \int_0^t F d\tau N(\tau) P_1(t - \tau). \quad (9b)$$

The last term in (9b) accounts for the loss of adatoms to the islands, treating islands as point-like objects. Since most islands are dimers in this regime, this is not a bad approximation. Here P_1 is given by P with the substitution $2D \rightarrow D$ in (B11). (In the eye of an adatom, the diffusion rate of another adatom is twice its value in the rest frame.)

Equations (9) can be solved by performing Laplace transforms. The results are given by, after the transformation,

$$N(p) = \frac{F}{p^2} \frac{FP(p)}{1 + 2FP(p) + F^2P(p)P_1(p)}, \quad (10a)$$

$$\rho(p) = \frac{F}{p^2} \frac{1}{1 + 2FP(p) + F^2P(p)P_1(p)}, \quad (10b)$$

where $P(p)$ is given by (B9). Here and elsewhere we use the same symbol for a function and its Laplace transform, but the distinction should always be clear from the context.

To obtain the inverse Laplace transform of (10) is not easy. However, by observing that

$$C(p) \equiv p^2 P(p)/(8D) \simeq -\pi/\ln(pe^\pi/64D) \quad (11)$$

is a slow-varying function in the regime $1/D \ll 1/p \ll t_1$, an approximate result can be obtained. Within the present degree of accuracy we can also write $P_1(p) \simeq 4DC(p)/p^2$. Treating $C(p)$ as a constant, the inverse transform can be readily carried out. The result is given by

$$N(t) \simeq (F/4DC)^{1/2} N^*(t\sqrt{4DFC}), \quad (12a)$$

$$\rho(t) = (F/4 DC)^{1/2} \rho^*(t \sqrt{4DFC}), \tag{12b}$$

where

$$N^*(x) = \frac{1}{\sqrt{4-2\sqrt{2}}} \sin(x\sqrt{2-\sqrt{2}}) - \frac{1}{\sqrt{4+2\sqrt{2}}} \sin(x\sqrt{2+\sqrt{2}}), \tag{13a}$$

$$\rho^*(x) = \frac{1}{2\sqrt{2-\sqrt{2}}} \sin(x\sqrt{2+\sqrt{2}}) - \frac{1}{2\sqrt{2+\sqrt{2}}} \sin(x\sqrt{2-\sqrt{2}}). \tag{13b}$$

The parameter C in (12) has a weak dependence on t . In view of (11), it is reasonable to write

$$C(t) \approx \pi/\ln(cDt), \tag{14}$$

where c is a constant.

Equation (12) is to be compared with equation (5) obtained from the rate-equations. For $x \ll 1$, $N^*(x)$ and $\rho^*(x)$ have the same leading-order behavior as $\tilde{N}(x)$ and $\hat{\rho}(x)$, respectively. The logarithmic corrections enter only through the scaling factors. Figure 5 is a modified version of figure 3, using the scaling parameters according to (12) and (14) with $c = 2$. The data collapse at early times is much better than in figure 3. The scaling functions (13) are shown by the dashed lines. They agree well with the data for $t \ll t_1$, but deviate from the collapsing curve as t_1 is approached.

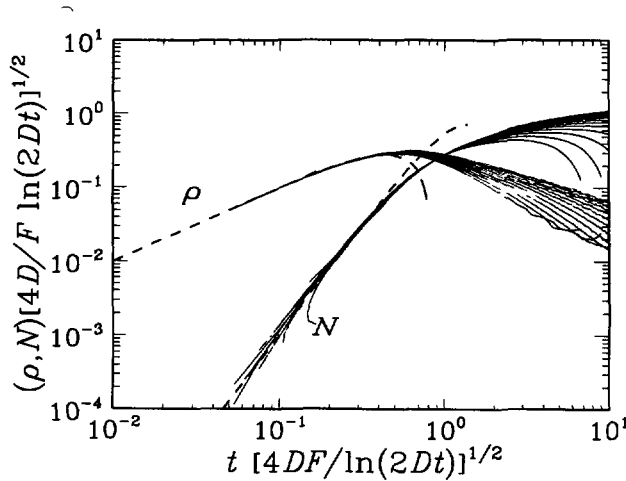


Fig. 5. — Replot of figure 3 using modified scaling parameters. Two dashed curves correspond to equation (13).

Equations (12) also implies that the time at which $N(t) = \rho(t)$ varies as $t \sim t_1 \ln^{1/2}(4D/F)$, in qualitative agreement with what we have seen in figure 3. The density of islands at this time is given by

$$N_1 = N_0(F/4D)^{1/2} \ln^{1/2}(2D/F), \tag{15}$$

where N_0 is a proportionality constant. Equation (15) is represented by the solid curve in figure 2, which compares better with the simulation data than a simple power-law.

4.2 PAIR FORMATION IN THE ISLAND GROWTH REGIME. — In contrast to the early time regime, the spatial distribution of adatoms for $t > t_1$ is much influenced by the presence of immobile islands which act as traps. The density of adatoms thus becomes inhomogeneous, being lower close to the islands. The inhomogeneity may possibly change the numerical factors in (1). However, the main correction to (1) comes again from improved estimates for the adatom-adatom and adatom-island collision rates considered below.

Since both ρ and N vary on a time scale much longer than the lifetime τ of adatoms in this regime, an adiabatic approximation which treats adatom diffusion in a fixed landscape of islands is in order. By definition we have $\rho = F\tau$. To create a new island, an adatom must make a collision with another adatom before its lifetime expires. This renders the following estimate for the pair-formation rate,

$$\frac{dN}{dt} \approx \frac{1}{2} F \rho P(\tau) \approx \frac{4 \pi D \rho^2}{\ln(c_1 D \rho / F)} \quad (16a)$$

A factor 1/2 is included to avoid double counting. As shown in figure 6a, equation (16a) is well-satisfied by the simulation data for $t_1 < t < t_2$. The left end of each curve corresponds to t close to t_2 , where coalescence starts to decrease the number of islands.

A second relation between ρ and N is needed to solve (16a). The adiabatic approximation applied to (1b) yields $\rho N \approx F/(4D)$. This relation is equivalent to $D\tau = (\ell/2)^2$ as one would get by equating the lifetime τ of an adatom to the diffusion time over a distance $\ell/2$. However, there is a logarithmic correction to this result when the dimension of islands is much smaller than their spacing. In appendix C we evaluate the mean density of adatoms in the steady-state for two different geometries, i) the islands are points arranged in a periodic array with a lattice spacing ℓ ; ii) the free space for adatom diffusion is a strip of width ℓ . Adatom-adatom collisions are ignored in the calculation. (This is reasonable because there are less adatoms than islands.) Within this approximation, the mathematics is reduced to that of the Coulomb problem, i.e., the density of adatoms satisfies the lattice Poisson equation with the boundary condition that the potential is zero at the sites next to the islands. We expect that the irregularity in the location and shape of the islands does not influence the average value of the adatom density away from the islands dramatically. For the average density of adatoms, the following results are obtained,

$$\rho \approx \begin{cases} (F\ell^2/2 \pi D)(0.306 + \ln \ell), & \text{case i),} \\ F\ell^2/12 D, & \text{case ii),} \end{cases}$$

respectively. The first formula is more accurate when the typical extension of islands R is much smaller than ℓ , while the second one is better when $R = \ell$. A simple interpolation of the two limits is given by

$$\rho \approx \frac{F\ell^2}{2 \pi D} \ln [\ell/R].$$

Writing $N = \ell^{-2}$, the above equation becomes

$$N\rho \approx -\frac{F}{4 \pi D} \ln [NR^2]. \quad (16b)$$

Figure 6b shows that this equation describes the simulation data well when $4D/F$ is sufficiently large and when t is not too close to t_1 . The left end of each curve, which corresponds to $t = t_1$, is significantly lower than the value given by (16b). This is because quasiequilibrium adatom population has not been established at this time.

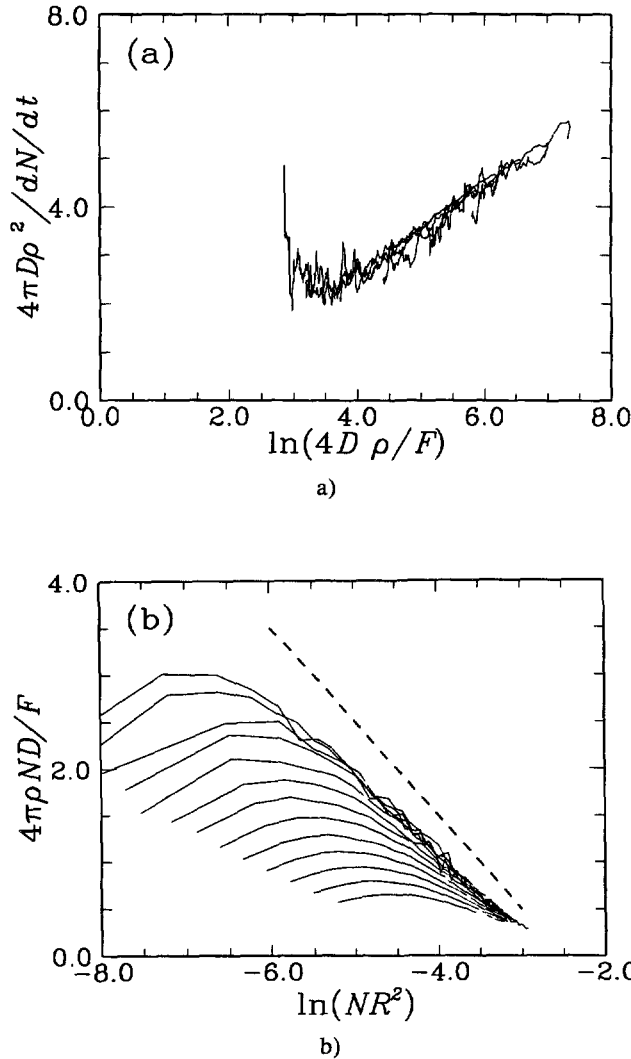


Fig. 6. — Pair formation rate and adatom density in the regime $t_1 < t < t_2$. Each curve corresponds to a given value of $4D/F \cong 1\,024$. (a) Scaled inverse pair formation rate versus adatom lifetime $\tau = \rho/F$. Time increases from right to left. (b) The product ρN versus area per island showing the logarithmic correction predicted by (16b). The noncollapsing part of the curves corresponds to $t \sim t_1$. A line of slope 1 is drawn for comparison.

To complete the calculation one has to determine the function $R(t)$. For compact islands, R^2 is roughly the average number of atoms per island. Since most atoms deposited are on the islands for $t > t_1$, we may write

$$NR^2 \approx Ft \quad (\text{compact islands}). \tag{17}$$

In this case equations (16) can be integrated to give

$$-N^3 \ln N \approx \frac{3F^2 t}{4D} \frac{1}{\pi} [\ln^2(Ft) - 2 \ln(Ft) + 2] + \text{Const}. \tag{18}$$

The constant of integration is determined by matching equation (18) to the value of N close to t_1 . The adatom density $\rho(t)$ can be obtained from equations (16b)-(18).

For fractal islands, equation (17) should be replaced by

$$NR^{d_f} = Ft/m_0 \quad (\text{fractal islands}), \quad (19)$$

where d_f is the fractal dimension of an island, and m_0 is a proportionality constant. Since R enters equation (16b) only through the logarithm, the result for $N(t)$ in this case is essentially the same as for compact islands, except that Ft inside the logarithms on the right-hand side of (18) is to be replaced by

$$NR^2 \approx Ft(4DFt^2)^{(2-d_f)/3} \quad (20)$$

The final expression for N is given by

$$N(t) = (F/4D)^{1/2} (3t\sqrt{4DF})^{1/3} \frac{\ln^{2/3}[Ft(4DFt^2)^{(2-d_f)/3}]}{[-(\pi/3)\ln(F^2t/4D)]^{1/3}}, \quad (21)$$

valid for $t_1 \ll t \ll t_2$.

It turns out that equation (21) does not compare well with our simulation data on a quantitative level. The problem has partly to do with the fact that equation (16b) holds only for $t \gg t_1$. In addition, we have omitted various constants that enter the logarithms, and the constant of integration in equation (18). Although equation (21) should give the leading order contribution to $N(t)$ for $t_1 \ll t \ll t_2$ when the beam is sufficiently weak, it seems not to be so accurate on a quantitative level even for $4D/F \sim 10^6$.

Finally, let us consider the maximum island density $N_{\max} = N(t_2)$. Using the condition that N_{\max} is reached at $R = \ell$ or $NR^2 \approx 1$, equation (20) yields,

$$Ft_2 \approx (F/4D)^{(2-d_f)/(4+d_f)} \quad (22)$$

Substituting (22) into (21) yields

$$N_{\max} \approx (F/4D)^{2/(4+d_f)} \ln^{-1/3}(4D/F). \quad (23)$$

This equation was obtained by Villain *et al.* [8] apart from the logarithmic correction.

5. Conclusion.

The main conclusion of this work is that a previous theory by Stoyanov and Kashchiev, based on a set of mean-field-type rate equations, offers a good description of island nucleation and growth in the submonolayer regime. The maximum density of islands N_{\max} decreases approximately as the 1/3 power of the ratio between layer completion time and the adatom hopping time, $4D/F$. However, significant deviations from the behavior predicted by the rate-equations are also observed. Some of these deviations can be explained quantitatively by including logarithmic corrections to the adatom-adatom and adatom-island collision rates.

When the islands are far apart from each other, they take a fractal shape. The fractal dimension of these islands are found to be comparable to that of DLA, in agreement with experiment [13]. By taking into account the fractal shapes, Villain *et al.* arrived at a modified formula for N_{\max} in the submonolayer regime. Our simulation shows that, when the final size of islands is not much larger than about ten lattice constants, other (logarithmic) corrections to the simple power-law predicted by the rate-equations are also important on a quantitative level.

Acknowledgements.

Many of the ideas on the interpretation of the simulation data grew out of an earlier collaboration with J. Villain and D. E. Wolf, to whom I am much indebted. Computations were performed on an IBM 3090 machine at the Forschungszentrum Jülich. The research is supported in part by DFG through SFB 341.

Upon completion of the paper I learnt from J. Villain that there exists a recent paper by Ghaisas and Das Sarma [30] where the functional dependence of the atomic diffusion length on the deposition rate in the (multilayer) steady-state was investigated.

Appendix A. Diffusion in the presence of traps.

Both pair formation and island growth can be thought of as a first-passage time problem for the adatoms. The mathematical problem of a single particle diffusing in the presence of traps can be formulated as follows. Let \mathfrak{T} be the set of traps, and $\Phi(\mathbf{r}, t)$ be the probability that the particle has coordinates \mathbf{r} at time t , we have

$$\frac{d\Phi(\mathbf{r}, t)}{dt} = \sum_{\mathbf{r}' \notin \mathfrak{T}} J(\mathbf{r} - \mathbf{r}') \Phi(\mathbf{r}', t) - \sum_{\mathbf{r}'} J(\mathbf{r}' - \mathbf{r}) \Phi(\mathbf{r}, t) (1 - \delta_{\mathbf{r}, \mathfrak{T}}). \quad (\text{A1})$$

Here $J(\mathbf{r} - \mathbf{r}') = J(\mathbf{r}' - \mathbf{r})$ is the hopping rate to a site \mathbf{r} from \mathbf{r}' , and $\delta_{\mathbf{r}, \mathfrak{T}} = 1$ for $\mathbf{r} \in \mathfrak{T}$ and 0 otherwise. Equation (A1) is generally known as the master equation for the diffusion process.

Introducing the Laplace transform

$$\phi(\mathbf{r}, p) = \int_0^{\infty} dt e^{-pt} \Phi(\mathbf{r}, t),$$

Equation (A1) can be rewritten as

$$\begin{aligned} p\phi(\mathbf{r}, p) + \sum_{\mathbf{r}'} J(\mathbf{r} - \mathbf{r}') [\phi(\mathbf{r}, p) - \phi(\mathbf{r}', p)] &= \\ &= \Phi(\mathbf{r}, 0) + \sum_{\mathbf{r}'} J(\mathbf{r} - \mathbf{r}') [\phi(\mathbf{r}, p) \delta_{\mathbf{r}, \mathfrak{T}} - \phi(\mathbf{r}', p) \delta_{\mathbf{r}', \mathfrak{T}}]. \end{aligned} \quad (\text{A2})$$

Equation (A2) can be solved formally by using the Green's function for the problem of no traps,

$$G(\mathbf{r}, p) = \int \frac{d^2k}{(2\pi)^2} \frac{e^{i\mathbf{k} \cdot \mathbf{r}}}{p + \lambda(\mathbf{k})}, \quad (\text{A3})$$

where \mathbf{k} is a wavevector in the Brillouin zone and

$$\lambda(\mathbf{k}) = \sum_{\mathbf{r}} (1 - e^{-i\mathbf{k} \cdot \mathbf{r}}) J(\mathbf{r}). \quad (\text{A4})$$

The result is given by

$$\phi(\mathbf{r}, p) = \phi(\mathbf{r}, p) \delta_{\mathbf{r}, \mathfrak{T}} + \sum_{\mathbf{R}} G(\mathbf{r} - \mathbf{R}, p) \Phi(\mathbf{R}, 0) - p \sum_{\mathbf{R} \in \mathfrak{T}} G(\mathbf{r} - \mathbf{R}, p) \phi(\mathbf{R}, p). \quad (\text{A5})$$

For $\mathbf{r} \in \mathcal{T}$, the above equation reduces to

$$\sum_{\mathbf{R} \in \mathcal{T}} G(\mathbf{r} - \mathbf{R}, p) \phi(\mathbf{R}, p) = \frac{1}{p} \sum_{\mathbf{R}} G(\mathbf{r} - \mathbf{R}, p) \Phi(\mathbf{R}, 0). \quad (\text{A6})$$

The complete solution to (A2) can be obtained by first solving the set of linear equations (A6) on \mathcal{T} and then using (A5).

Appendix B. Adatom-adatom collision.

In relative coordinates, adatom-adatom collision can be described by equation (A1) with $J'(\mathbf{r}) = 2J(\mathbf{r})$. Since two adatoms form a pair when they become nearest neighbors, the diffusion process is stopped when \mathbf{r} reaches any of the four nearest neighbors of the origin. These four sites make up of the set \mathcal{T} . In the following we shall focus on the case

$$J'(\mathbf{r} - \mathbf{r}') = \begin{cases} 2D, & \text{if } \mathbf{r} \text{ and } \mathbf{r}' \text{ are nearest neighbors;} \\ 0, & \text{otherwise.} \end{cases} \quad (\text{B1})$$

Here D is the diffusion constant for a single particle.

The probability that two adatoms separated by a distance \mathbf{R} at $t = 0$ have formed a pair at a later time t is given by

$$P_{\mathbf{R}}(t) = \sum_{\mathbf{r} \in \mathcal{T}} \Phi_{\mathbf{R}}(\mathbf{r}, t), \quad (\text{B2})$$

with the condition that $\Phi_{\mathbf{R}}(\mathbf{r}, 0) = \delta_{\mathbf{r}, \mathbf{R}}$. We are interested in calculating the probability $\Pi(\rho, t)$ that an atom landed at $t = 0$ forms a pair with any of the preexisting adatoms of uniform density ρ within a time interval t . In the low density limit and for not too large t it is reasonable to write

$$\Pi(\rho, t) = \sum_{\mathbf{R}} P_{\mathbf{R}}(t) = \rho P(t), \quad (\text{B3})$$

with \mathbf{R} being a set of randomly distributed points of density ρ . Here

$$P(t) = \sum_{\mathbf{r} \in \mathcal{T}} \Phi(\mathbf{r}, t), \quad (\text{B4})$$

with $\Phi(\mathbf{r}, t)$ being a solution to (A1) under the initial condition $\Phi(\mathbf{r}, 0) = 1$.

The Laplace transform of $P(t)$ can be obtained by summing both sides of equation (A6) over $\mathbf{r} \in \mathcal{T}$ and using the condition $\sum_{\mathbf{R}} G(\mathbf{r} - \mathbf{R}, p) = 1/p$,

$$P(p) = \sum_{\mathbf{r} \in \mathcal{T}} \phi(\mathbf{r}, p) = \frac{4}{p^2} \frac{1}{G_0(p) + 2G_1(p) + G_2(p)}, \quad (\text{B5})$$

where

$$\begin{aligned} G_0(p) &= \int_{-\pi}^{\pi} \frac{dk_1}{2\pi} \int_{-\pi}^{\pi} \frac{dk_2}{2\pi} \frac{1}{p + 4D(2 - \cos k_1 - \cos k_2)}, \\ G_1(p) &= \int_{-\pi}^{\pi} \frac{dk_1}{2\pi} \int_{-\pi}^{\pi} \frac{dk_2}{2\pi} \frac{\cos(k_1 + k_2)}{p + 4D(2 - \cos k_1 - \cos k_2)}, \\ G_2(p) &= \int_{-\pi}^{\pi} \frac{dk_1}{2\pi} \int_{-\pi}^{\pi} \frac{dk_2}{2\pi} \frac{\cos(2k_1)}{p + 4D(2 - \cos k_1 - \cos k_2)} \end{aligned} \quad (\text{B6})$$

The above expressions can be reduced to complete elliptic integrals. In particular,

$$G_0(p) = \frac{2}{\pi} \frac{1}{8D+p} K\left(\frac{1}{1+(p/8D)}\right), \tag{B7}$$

where $K(k)$ is the elliptic integral of the first kind. Using the symmetry properties of the integrals in (B6), we write

$$\begin{aligned} G_0(p) + 2G_1(p) + G_2(p) &= \int_{-\pi}^{\pi} \frac{dk_1}{2\pi} \int_{-\pi}^{\pi} \frac{dk_2}{2\pi} \frac{(\cos k_1 + \cos k_2)^2}{p + 4D(2 - \cos k_1 - \cos k_2)} \\ &= \frac{1}{2D} \left(1 + \frac{p}{8D}\right) \left[\frac{2}{\pi} K\left(\frac{1}{1+(p/8D)}\right) - 1 \right]. \end{aligned} \tag{B8}$$

Substituting (B8) into (B5) yields

$$P(p) = \frac{8D}{p^2 \left(1 + \frac{p}{8D}\right)} \frac{1}{\frac{2}{\pi} K\left(\frac{1}{1+(p/8D)}\right) - 1} \tag{B9}$$

The behavior of $P(t)$ at large t is determined by $P(p)$ at small p . Using the expansion of $K(\sqrt{1-k'^2})$ for $k' \ll 1$, $K(\sqrt{1-k'^2}) = \ln(4/k') + O(k'^2 \ln k')$, we obtain,

$$P(p) = \frac{8\pi D}{p^2} \frac{1 + O(p)}{-\ln(pe^\pi/64D)} \tag{B10}$$

The inverse Laplace transform of (B10) is given by, for $Dt \gg 1$,

$$P(t) \approx 8\pi Dt / \ln(32e^{-\pi}Dt). \tag{B11}$$

We have not attempted to evaluate the coefficient inside the logarithm accurately.

Appendix C. Steady-state in a periodic array of traps.

Let us now consider adatom diffusion with \mathfrak{T} being a periodic array of points commensurate with the underlying lattice. Pair formations are ignored.

Since (A1) is linear, we can also think of $\Phi(\mathbf{r}, t)$ as the density profile of an ideal gas of adatoms diffusing in the presence of traps. Let us now consider the time evolution of such an ideal gas of uniform density at $t = 0$. For simplicity we take $\Phi(\mathbf{r}, 0) = 1$. Due to the translational symmetry of the problem, (A6) can be easily solved for $\mathbf{r} \in \mathfrak{T}$,

$$\phi(\mathbf{r}, p) = \frac{1}{p^2} Q(p), \tag{C1}$$

with

$$Q^{-1}(p) = \sum_{\mathbf{r} \in \mathfrak{T}} G(\mathbf{r}, p) = \frac{1}{M} \sum_{\mathbf{q}} \frac{1}{p + \lambda(\mathbf{q})} \tag{C2}$$

Here and elsewhere the sum over \mathbf{q} is restricted to the reciprocal lattice vectors of \mathfrak{T} which lie inside the Brillouin zone of the original lattice, and M is the number of such wavevectors. Substituting (A14) into (A5) yields, for $\mathbf{r} \notin \mathfrak{T}$,

$$\phi(\mathbf{r}, p) = \frac{1}{p} - \frac{Q(p)}{pM} \sum_{\mathbf{q}} \frac{e^{i\mathbf{q} \cdot (\mathbf{r} - \mathbf{R}_0)}}{p + \lambda(\mathbf{q})}, \tag{C3}$$

where \mathbf{R}_0 is any point in \mathfrak{T} . Obviously $\phi(\mathbf{r}, p)$ has the translational symmetry of \mathfrak{T} .

The adatom density at a constant deposition rate F can be obtained by integrating $\Phi(\mathbf{r}, t)$ over t ,

$$\rho(\mathbf{r}, t) = \int_0^t F dt' \Phi(\mathbf{r}, t'). \quad (\text{C4})$$

The Laplace transform of $\rho(\mathbf{r}, t)$ is thus given by

$$\rho(\mathbf{r}, p) = \frac{F}{p} \frac{Q(p)}{pM} \sum_{\mathbf{q}} \frac{1 - e^{i\mathbf{q} \cdot (\mathbf{r} - \mathbf{R}_0)}}{p + \lambda(\mathbf{q})} \quad (\text{C5})$$

In the limit $p \rightarrow 0$, $Q(p) \approx Mp$, and $\rho(\mathbf{r}, p) \approx \rho_s(\mathbf{r})/p$, with

$$\rho_s(\mathbf{r}) = F \sum_{\mathbf{q} \neq 0} \frac{1 - e^{i\mathbf{q} \cdot (\mathbf{r} - \mathbf{R}_0)}}{\lambda(\mathbf{q})} \quad (\text{C6})$$

being the steady-state adatom density. The average density of adatoms is given by

$$\bar{\rho}_s = F \sum_{\mathbf{q} \neq 0} \frac{1}{\lambda(\mathbf{q})} \quad (\text{C7})$$

Let us now consider two special examples of \mathfrak{T} , with $\lambda(q_1, q_2) = 2D(2 - \cos q_1 - \cos q_2)$. In the first example we take \mathfrak{T} to be a square lattice with a lattice constant ℓ times that of the underlying lattice. The sum over $\mathbf{q} = (q_1, q_2)$ is limited to $q_1 = 2\pi m/\ell$, $q_2 = 2\pi n/\ell$, $m, n = 0, \dots, \ell - 1$. Equation (C6) can now be written as

$$\begin{aligned} \bar{\rho}_s &= \frac{F}{2D} \left[\sum_{m=1}^{\ell-1} \frac{1}{1 - \cos(2\pi m/\ell)} + \sum_{n=1}^{\ell-1} \sum_{m=0}^{\ell-1} \frac{1}{2 - \cos(2\pi m/\ell) - \cos(2\pi n/\ell)} \right] \\ &= \frac{F\ell^2}{2\pi D} \left[\ln \ell + \frac{\pi}{6} + \gamma + \ln \frac{\sqrt{2}}{\pi} + 2 \sum_{n=1}^{\infty} \frac{1}{n} \frac{1}{e^{2\pi n} - 1} + O(1/\ell) \right]. \end{aligned} \quad (\text{C8})$$

Here $\gamma = 0.5772\dots$ is the Euler constant.

In the second example we let \mathfrak{T} to be a set of equally spaced lines of distance ℓ parallel to the x -axis. In this case the sum in (C7) is taken over $q_1 = 0$ and $q_2 = 2\pi n/\ell$, $n = 1, \dots, \ell - 1$. Using the identity

$$\sum_{n=1}^{\ell-1} \frac{1}{1 - \cos(2\pi n/\ell)} = \frac{\ell^2 - 1}{6},$$

we obtain

$$\bar{\rho}_s = \frac{F(\ell^2 - 1)}{12D} \quad (\text{C9})$$

This result can also be obtained by solving the steady-state equation for $\rho_s(\mathbf{r})$ directly [31].

References

- [1] For reviews of recent development see, e.g., Kinetics of Ordering and Growth at Surfaces, M. Lagally Ed. (Plenum, New York, 1990) and references therein.
- [2] VENABLES J. A., SPILLER G. D., HANBÜCKEN M., *Rep. Prog. Phys.* **47** (1984) 399.
- [3] STOYANOV S. and KASHCHIEV D., in Current Topics in Materials Science, Vol. 7, E. Kaldis Ed. (Amsterdam, North-Holland, 1981) p. 69.
- [4] VILLAIN J., WOLF D. E. and PIMPINELLI A., *Comm. Cond. Matt. Phys.* **16** (1992) 1.
- [5] FUENZALIDA V., *Phys. Rev. B* **44** (1991) 10835.
- [6] LUSE C. N., ZANGWILL A., VVEDENSKY D. D. and WILBY M. R., *Surf. Sci. Lett.* **274** (1992) L535.
- [7] STOYANOV S. and MICHAÏLOV M., *Surf. Sci.* **202** (1988) 109.
- [8] VILLAIN J., PIMPINELLI A., TANG L.-H. and WOLF D. E., *J. Phys. I France* **2** (1992) 2107.
- [9] VILLAIN J., *J. Phys. I France* **1** (1991) 19.
- [10] DE MIGUEL J. J., SÁNCHEZ A., CEBOLLADA A., GALLEGO J. M., FERRÓN J. and FERRER S., *Surf. Sci.* **189/190** (1987) 1062.
- [11] IRISAWA T., ARIMA Y. and KURODA T., *J. Cryst. Growth* **99** (1990) 491.
- [12] MO Y. M., KLEINER J., WEBB M. B. and LAGALLY M. G., *Phys. Rev. Lett.* **66** (1991) 1998 ; *ibid.* **69** (1992) 986 ;
PIMPINELLI A., VILLAIN J. and WOLF D. E., *ibid.* **69** (1992) 985.
- [13] HWANG R. Q., SCHRÖDER J., GÜNTHER C. and BEHM R. J., *Phys. Rev. Lett.* **67** (1991) 3279.
- [14] NEAVE J. H., DOBSON P. J., ZHANG J. and JOYCE B. A., *Appl. Phys. Lett.* **47** (1985) 100.
- [15] EDWARDS S. F. and WILKINSON D. R., *Proc. R. Soc. London, Ser. A* **381** (1982) 17.
- [16] KARDAR M., PARISI G. and ZHANG Y.-C., *Phys. Rev. Lett.* **56** (1986) 889.
- [17] FAMILY F. and VICSEK T., Dynamics of Fractal Surfaces (World Scientific, Singapore, 1991).
- [18] WOLF D. E. and VILLAIN J., *Europhys. Lett.* **13** (1990) 389.
- [19] DAS SARMA S. and TAMBORENEA P. I., *Phys. Rev. Lett.* **66** (1991) 325 ;
LAI Z.-W. and DAS SARMA S., *Phys. Rev. Lett.* **66** (1991) 2324.
- [20] TANG L.-H. and NATTERMANN T., *Phys. Rev. Lett.* **66** (1991) 2899.
- [21] SIEGERT M. and PLISCHKE M., *Phys. Rev. Lett.* **68** (1992) 2035.
- [22] KESSLER D. A., LEVINE H. and SANDER L. M., *Phys. Rev. Lett.* **69** (1992) 100.
- [23] ZANGWILL A., LUSE C. N., VVEDENSKY D. D. and WILBY M. R., *Surf. Sci. Lett.* **247** (1992) L529.
- [24] HERRMANN H. J., *Phys. Rep.* **136** (1986) 153.
- [25] MEAKIN P., *Phys. Rev. Lett.* **51** (1983) 1119 ;
KOLB M., BOTET R. and JULLIEN R., *ibid.* **51** (1983) 1123.
- [26] ERNST H.-J., FABRE F. and LAPUJOLADE J., *Phys. Rev. Lett.* **69** (1992) 458.
- [27] HOSHEN J. and KOPELMAN R., *Phys. Rev. B* **14** (1976) 3438.
- [28] WITTEN T. A. and SANDER L. M., *Phys. Rev. Lett.* **47** (1981) 1400.
- [29] MONTROLL E. W. and WEISS G. H., *J. Math. Phys.* **6** (1965) 167 ;
See also the review article by HAUS J. W. and KEHR K. W., *Phys. Rep.* **150** (1987) 263.
- [30] GHASIS S. V. and DAS SARMA S., *Phys. Rev. B* **46** (1992) 7308.
- [31] BURTON W. K., CABRERA N. and FRANK F. C., *Philos. Trans. R. Soc. London, Ser. A* **243** (1951) 299 ;
VILLAIN J., private communication.